Calibration of the absolute light–yield of various scintillator screens for electron bunch charge determination in laser–plasma accelerators

Thomas Kurz,[1,2,3,a)] Jakob Matthias Krämer,[1,3] Jurjen Pieter Couperus,[1,3] Hao Ding,[2,4] Stefan Kuschel,[5,6] Alexander Köhler,[1,3] Omid Zarini,[1,3] Dominik Hollatz,[5,6] David Schinkel,[5,6] Richard D'Arcy,[7] Jan Patrick Schwinkendorf,[7,8] Arie Irman,[1] Ulrich Schramm,[1,3] and Stefan Karsch[2,4]

[1] *Helmholtz-Zentrum Dresden – Rossendorf, Bautzner Landstraße 400, D-01328 Dresden, Germany*

[2] *Ludwig–Maximilians–Universität München, Am Coulombwall 1, D-85748 Garching, Germany*

[3] *Technische Universität Dresden, D-01069 Dresden, Germany*

[4] *Max–Planck–Institut für Quantenoptik, Hans-Kopfermann-Straße 1, D-85748 Garching, Germany*

[5] *Helmholtz–Institut Jena, Fröbelstieg 3, D-07743 Jena, Germany*

[6] *Friedrich–Schiller–Universität Jena, Fürstengraben 1, D-07743 Jena, Germany*

[7] *Deutsches Elektronen–Synchrotron, Notkestraße 85, D-22607 Hamburg, Germany*

[8] *Universität Hamburg, Jungiusstraße 9, D-20355 Hamburg, Germany*

(Dated: 15 August 2017)

This article gives information about the absolute light yield of different scintillating screens used in current laser-plasma experiments. The calibration was designed to investigate the light/charge–conversion and saturation effects of different screens. In order to reach the necessary electron fluence, the screens were excited by a weakly focused electron beam, generating high peak charge density up to $20\,\mathrm{nC/mm^2}$ delivered from the ELBE linear accelerator at the Helmholtz-Zentrum in Dresden – Rossendorf. A three orders of magnitude linearity in light yield to charge conversion was found followed by a saturation area starting in the range of $\mathrm{nC/mm^2}$. Furthermore for a specific type of scintillator long–term stability test were done. A significant decrease of the scintillation efficiency with conditions comparable to a LPA–experiment was found. Also included is a description for a new type of reference light source performing the screen cross–calibration.

Usage: Secondary publications and information retrieval purposes.

PACS numbers: May be entered using the \pacs{#1} command.

Structure: You may use the `description` environment to structure your abstract; use the optional argument of the \item command to give the category of each item.

PACS numbers: Valid PACS appear here

I. INTRODUCTION

Since their theoretical predication in 1979 by Tajima and Dawson[1], laser-plasma wakefield accelerators (LWFA) have seen tremendous progress. These accelerators can operate with accelerating gradients of up to several hundreds of $\mathrm{GeV\,m^{-1}}$, three to four orders of magnitude higher than in conventional accelerators. Recent advancement in both the understanding of the acceleration mechanism as well as development of state of the art laser–systems, which are now able to operate in the petawatt–regime[2,3], make it possible to accelerate quasi–monoenergetic[4–6] electron bunches containing charges of several hundred pC to energies in the GeV–range[7–9]. Providing ultra–short bunch lengths of only a few femtoseconds, these accelerators can deliver several tens of kA peak-current [10?] making them them ideal drivers for next-generation compact light-sources cover-

ing high-field THz[?,?], high-brightness X-ray[11,12] and γ–ray[13,14] sources, compact FELs[15? –18] and laboratory-size beam-driven plasma accelerators[19,20].

However, laser plasma accelerators (LPAs) are still a developing field. Compared to conventional accelerators many challenges remain, both in beam quality as well as in shot-to-shot stability. In order to further improve the performance of LPAs, it is necessary to understand the accelerator dynamics and to be able to resolve shot-to-shot fluctuations. Therefore, a well suited single-shot electron diagnostic is required which resolves charge, energy and divergence over a large parameter range.

Typically a combination of a broad energy-range dipole magnet, which maps electron energy to position in the dispersive plane, is used in combination with a scintillation screen imaged onto a camera for charge diagnostic. This screen generally covers an area in the order of hundreds of $\mathrm{cm^2}$ to monitor the relevant parameter range. Established techniques at conventional accelerators such as Faraday cups and integrating current transformers (ICT) aren't reasonable alternatives, as they are not capable of delivering the required energy–resolved

charge information.

These scintillation screens consist of a 10 μm to 100 μm–thick layer of powdered rare earth phosphor (Gd2O2S:TB), that converts electron energy into visible light. The process is dominated by fluorescence and has a life–time of approximately 1 ms. This short lifetime enables single shot diagnostic at relevant LPA repetition rates (up to 10 Hz). In contrast, imaging plates, which deliver good energy resolution and a high dynamic range[21–24], suffer from a long read-out time. Scintillating screens are commercially available, often under the trade name LANEX, and marketed for X-ray detection. Generally no electron–photon conversion efficiency is specified and careful calibration is required before application.

In this work we report on the absolute charge calibration of several commercially available scintillating screens. These calibrations are performed under conditions close to those found in LWFA experiments, providing a significant improvement over previous reported calibration values by Buck et al.[25]. Additionally we report on several other relevant effects. In section III B the non–linear response of the scintillator at high electron flux is presented. Crucial information on the long term stability and damage resistivity of the screens are reported in section III C.

The insights found in this work will have a significant impact on the application of scintillating screens as a charge diagnostic at LPAs. The absolute calibration presented here has significant improvements compared to previous work and will act as a new standard in the field.

II. EXPERIMENTAL SETUP

The setup for the absolute charge calibration of the scintillation screens is illustrated in Fig. 1. The measurement was performed at the ELBE linear accelerator (LINAC) at the Helmholtz-Zentrum Dresden – Rossendorf. Sub–10 ps long electron bunches with charges up to 50 pC are accelerated to an energy of 23 MeV at 13 MHz repetition rate. For generating higher charges, the accelerator is operated in multiple bunch mode with tunable length. The temporal delay of the single bunches within this pulse–train is 77 ns. The total charge of this train is deposited on the screen in a short period compared to the lifetime of the excited state (≈ 1 ms) in the scintillator[26]. Ideally the scintillator–calibration takes place at relevant energies (≥ 200 MeV), but the power of the linear accelerator is limited to 23 MeV. However, simulations show that the energy deposition of the electrons inside the photo–luminescent layer is almost independent of their kinetic energy above a threshold–value of 3 MeV [22,27,28]. Thus the calibration results obtained at 23 MeV can be used to determine the charge in an experiment with highly relativistic electrons, i.e. laser wakefield acceleration even though the energy is one order of magnitude lower than in LPA experiments.

The electron beam is focused by magnetic quadrupoles

to a full width at half maximum (FWHM)–beam size of 6 mm^2 to 7 mm^2 at the target. This leads to charge densities up to 20 nC/mm^2 which are necessary to study saturation effects in the active layer of the scintillator. Immediately before interaction with the screen, the charge of each electron bunch is measured by an integrated current transformer (ICT–082–070–05:1–VAC, Bergoz Instrumentation, France). The ICT pulses were amplified by a factor of 56 (Pulse Amplifier Coaxial ZPUL–30P, Mini Circuits, USA) and recorded by a high quality oscilloscope (2GHz RTE 1204, Rhode&Schwarz, Germany).

After passing the ICT, the electrons interact with the screen. In the active layer of the screen, phosphor atoms are excited by the incoming electrons and radiate photons while relaxing back into the ground state. The light emission distribution of the screens follows approximately Lambertian law[29]. The screens were mounted on a rotating target wheel which was aligned $(22 \pm 1)°$ relative to the electron beam. The deflector mirror is mounted out of the beam–axis to avoid any background from optical transition radiation (OTR). The emitted photons with a peak wavelength λ_{peak} of 546 nm are reflected by a silver mirror (Thorlabs, PF20-03-P01) under $(34 \pm 1)°$ to a 12–bit CCD–camera (Basler, acA1300-30gm) equipped with a high–definition tele–objective. Due to the alignment of the mirror the camera looks perpendicularly onto the screens which maximizes the light emission onto the CCD–chip according to Lambertian law.

In front of the camera–lens, a wheel equipped with a series of ND–filters ranging from ND0.5 to ND4.0 is placed generating a dynamic range of 7 orders of magnitude. In order to minimize the measurement uncertainties, the filters were calibrated precisely (below 0.5% uncertainty) using a well–calibrated photo–spectrometer (Cary® 50 UV-VIS). The effective aperture in our optical detection system was $(3.18 \pm 0.07) \times 10^{-3}$ sr defined by an aperture with (22.96 ± 0.05) mm mounted at a distance of (361 ± 4) mm to the target. For this small angle, the Lambertian distribution of the screen can be ignored. Additionally an optical fiber (M200L02S-A, Thorlabs) connected to a spectrometer (HR4000, Ocean Optics) is implemented in the setup in order to determine the spectrum of the scintillation screens and the constant light sources. The fiber is placed on a linear motor to switch quickly between calibration and spectrum measurements.

III. RESULTS

A. Absolute charge calibration

The absolute calibration (total photons/pC/sr) is generally used to benchmark scintillators that are used as the charge diagnostic in LPAs. Therefore, we have calibrated our optical detection system in order to determine the absolute amount of photons/sr emitted by the scintillator. Together with a precise knowledge (5% uncertainty) of the LINAC's bunch charge we are able to
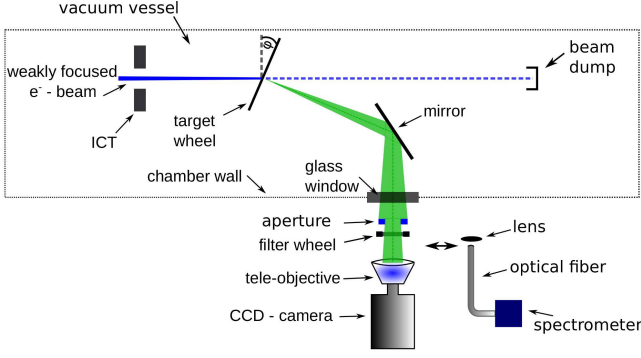
FIG. 1. Setup for absolute charge calibration of scintillation screens: ICT measures the charge of the electron beam. Six different screens with an angle of 22° relative to the incoming electron beam were mounted on a filter wheel and optically imaged via a silver mirror onto a CCD–chip. In order to generate the desired dynamic range a set of ND–filters was placed in front of the camera.
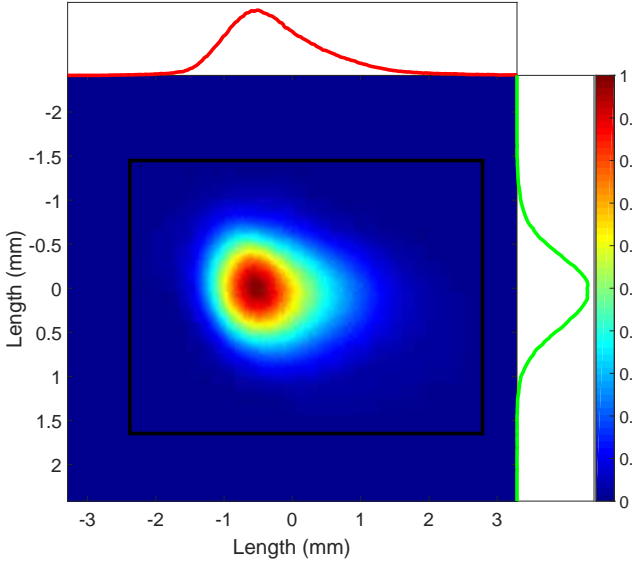

FIG. 2. Image of electron bunch recorded by CCD–sensor. The rectangle marks the region of interest (ROI) which was used for the analysis. The two curves indicate the line–out of the electron bunch through its peak in horizontal and vertical direction. The area of the bunch at FWHM is $\approx 6\,\mathrm{mm}^2$.

measure the absolute scintillation efficiency in case of an excitation with relativistic electrons.

A representative image of an electron bunch that was recorded during the calibration is shown in Fig. 2. The brightness of the scintillator is measured as the integrated CCD–counts in the ROI and corrected for the background from the camera and the accelerator (darkcurrent). Accordingly the absolute response of the scintillator, i.e. the total number of photons N_{photon} emitted by the scintillator into an area of one steradian per inci-

dent electron charge Q_{electron} can be described as

$$\frac{N_{\mathrm{photon}}}{Q_{\mathrm{electron}}} = N_{\mathrm{count}} \cos(\varphi)\beta^{-1}\Omega^{-1}Q_{\mathrm{electron}}^{-1} , \quad (1)$$

where N_{count} describes the total number of counts in the ROI of the raw image. φ is the angle between the electron beam and the normal vector of the scintillator's surface. The cosine corrects the photon signal recorded by the CCD–camera for the incidence angle of the electrons since they have an elongated interaction length scaling with $\cos(\varphi)^{-1}$. Ω symbolizes the effective collection angle in units of steradian. Finally, β denotes the efficiency of the entire detection system, i.e. the probability for a photon created at the source, to travel through the optical beamline, reaching the CCD–chip and be converted to a count by the analog–to–digital converter. For completeness, β can be disassembled in its individual parts. The transmission of the off-axis mirror at the specific wavelength is $(97 \pm 1)\,\%$, the window of the vacuum–chamber transmits $(91.3 \pm 0.5)\,\%$ of the incoming light and the objective images 88 ± 1 out of 100 impinging photons on the chip. The photon–to–count conversion efficiency of $(32.8 \pm 1.7)\,\%$ of the CCD–chip (Sony ICX445) and its associated readout-electronics was determined separately using a green laser and a reference detector (XLP12-3SH2-D0, Gentec International, Canada).

The response functions for the different screens are shown in Fig. 3. The curves show a linear behavior up to a threshold caused by saturation and degeneration effects (Sec. III B, III C). In order to determine the calibration value for the absolute response of the different scintillator, a linear fit has been applied to all datapoints within the linear region. The resulting calibration values are shown in Table I. The error of the values was determined using the method of Gaussian error propagation.

B. Saturation effects

Beyond the linear region of the calibration curves, the signal/charge–ratio gets non–linear due to a saturation in the active layer of the scintillator. Saturation occurs because the probability that certain atoms are excited multiple times before relaxing back into the ground state increases with the charge density. Birk's law is used to fit the response curve of the scintillator:

$$\rho_{\mathrm{scint}} = \frac{\rho_{\mathrm{ICT}}}{1 + B\rho_{\mathrm{ICT}}} , \quad (2)$$

where the fit parameter B is the Birk's constant. Here, ρ_{ICT} is the applied charge density which is determined by the electron bunch charge recorded by the ICT and the beam profile of the scintillator in the linear region. Assuming a constant bunch profile, we extrapolate ρ_{ICT} into the saturated regime using the charge information given by the ICT. ρ_{scint} is the charge density detected by the scintillator. The saturation value ρ_{sat} is defined as

TABLE I. Calibration values for different scintillation screens in the linear range: The absolute light yield per incident electrons (left column) and the saturation threshold (center column) as well as the resulting fit parameter (right column).

Screen	Absolute fluorescence efficiency $(10^9$ ph/sr/pC$)$	Saturation threshold $(10^3$ pC/mm$^2)$	Birk's constant $(10^{-5}$ mm^2/pC$)$
KODAK BioMAX MS	7.7 ± 1.3	4.2 ± 0.2	5.9 ± 0.3
Cawo OG BACK	5.8 ± 1.0	5.0 ± 0.3	5.0 ± 0.3
Cawo OG FRONT	3.7 ± 0.7	4.9 ± 0.3	5.1 ± 0.3
Konica Minolta OG 400	3.7 ± 0.7	5.2 ± 0.4	4.8 ± 0.4
Carestream Lanex Regular	3.1 ± 0.6	5.1 ± 0.3	4.9 ± 0.3
Kodak Lanex Fine	1.0 ± 0.2	9.6 ± 0.5	2.6 ± 0.3

the peak charge density, at which the scintillation signal has dropped down to 80% compared to the linear behavior. This arbitrary measure is chosen such that the saturation effect can be clearly distinguished from measurement uncertainties in the linear case. Fig. 4 shows a saturated response for Kodak BioMAX MS of the scintillation peak signal with increasing electron peak charge density. The black dashed line shows the linear correlation of ρ_{scint} and ρ_{ICT}, while the red curve indicates the fit along the measured data. We observe significant non–linearities in the saturation curve in the range of nC/mm^2. The resulting threshold values and the fit parameter B for the different screens are shown in table I. It should be noted, the experimental implementation of the setup potentially underestimates this effect. For the highest applied charges, the temporal length of the pulse train becomes significantly high compared to the life–time of the excited state. Electrons in the back of the bunch have an enhanced probability to excite an atom that has already relaxed back and thus add less to saturation. This effect has been included as an increased uncertainty towards lower response and is only relevant for the last two data–points.

Besides reversible saturation is visible additionally permanent degeneration comes into play (see Sec. III C). Reference measurements with a low charge of 60 pC after each increment of the bunch charge during the calibration were performed to get a reasonable estimation for the correction factor in the saturation curve. The values in Table I and Fig. 4 are corrected for this damage.

C. Long–term stability tests

A reliable performance of the particle detector is a very crucial issue in a LPA because it ensures the correct determination of the bunch charge. Up to now a constant light yield factor (see Sec. III A) over time was assumed but never experimentally confirmed. We have tested non–reversible degeneration or artificial aging effects of the phosphor layer caused by the electron dose applied to the screens during a dedicated long term run. The experimental parameters were chosen such to represent LWFA–conditions as close as possible. Every second, the screen was irradiated by an electron bunch with

a charge of 100 pC for a measurement–time of 90 min. The FWHM–bunch area was kept at 6 mm^2 to get realistic mean electron densities at the target on the order of 9 pC/mm^2. Fig. 5 shows the fluorescence signal as a function of the applied cumulated electron charge density over time. A significant drop of 9 % in the emitted scintillation efficiency over time can be observed.

The temporal evolution of the fluorescence efficiency during a different long term test than the discussed above one is plotted in Fig. 6. First, the scintillator shows the same decay. For instance, the beam profile for a shot onto the scintillator at 50 nC/mm^2 is illustrated in Fig. 6. At a cumulative charge density of around 52 nC/mm^2 the response function exhibits a sharp peak at which the screen lights up brightly with a hole in its center. Afterwards the screen is permanently damaged and approximately three times darker than before. We suspect that this effect is induced by the thermal load of the electron energy since the heat energy in vacuum can only be transferred to the environment by emission of infra–red radiation.

IV. DISCUSSION

We present an absolute charge calibration measurement and linearity and long stability test for various scintillators used in current laser accelerators as the charge for relativistic electron detection with a dynamic range and ac- curacy that has not been done so far to our knowledge There were already former calibration studies of scintillators some years ago by Glinec et al.[28], Buck et al.[25] and Nakamura et al.[30]. Among those the work of Buck et al.[25] is commonly considered as the reference for charge determination in the LPA–community because they present calibration values for many different scintillation screens with high precision. However, their calibration is performed under conditions far away from those typically found in laser accelerators and some of the screens are not commercially available anymore. Thus the work presented here provides an update for the absolute calibration values of scintillators using a significantly improved setup. In order to compare the results, we calculated the scintillation efficiency based on the experimental values published by Glinec et al.[28]. It leads to an absolute conversion efficiency for KODAK Lanex Fine of
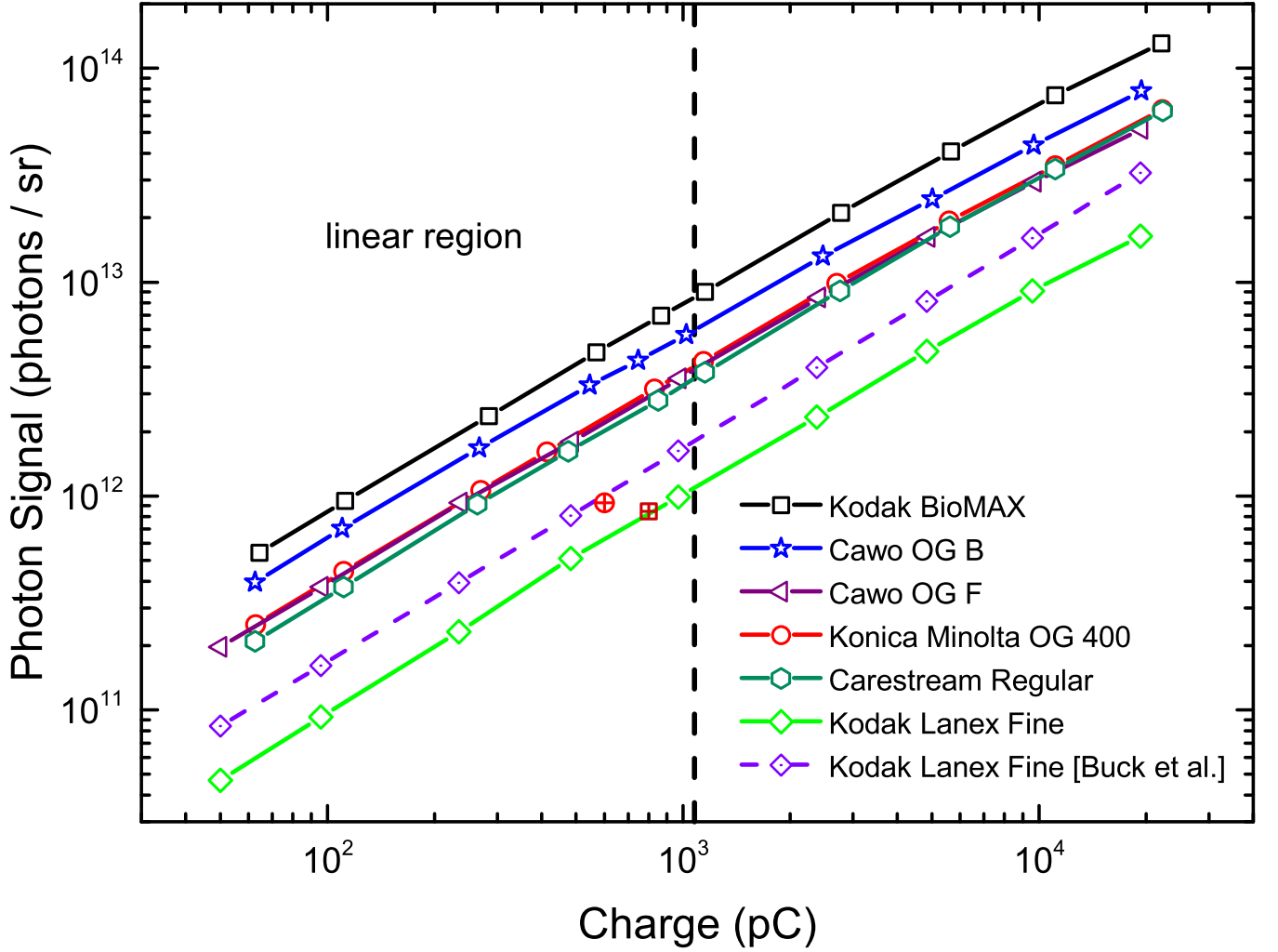
FIG. 3. (Color) Absolute charge calibration of six different scintillation screens. The linearity hypothesis is valid up to a certain charge density threshold. Beyond this threshold, nonlinear saturation effects start to play a role in the photon response. The dashed line indicates a calibration curve for Kodak Lanex Fine from Buck et al.[25] . Additionally two reference data–points for Kodak Lanex Fine are included. The red circle is determined by a calculation based on a Monte–Carlo–Simulation reported in Glinec et al.[28] as referenced in Buck et al. The red square was deduced from the full set of experimental results given by Glinec et al..

$(1.05 \pm 0.09) \times 10^9$ ph/sr/pC which shows a good agreement to our value of $(1.0 \pm 0.2) \times 10^9$ ph/sr/pC. When using a Cawo OG screen it also matters which surface is irradiated. The signal emitted by the back side is 50% higher than the front side–signal.

The absolute calibration has the disadvantage that it depends on the geometry of the optical detection system. We found that a smart way to avoid the afore mentioned error–sources and to simplify the determination of the electron bunch charge in a laser–plasma experiment is the cross–calibration of the scintillator with a constant light source. In particular, we implemented a gaseous tritium light source (GTLS) and an LED–based diffused green radiator. The LED–source has an extended life–time such that the cross–calibration can be applied correctly for many years. In certain scenarios the GTLS are still preferred due to their small size and vacuum compatibility. In such cases the LED–source acts as a master light source to which tritium light sources can be cross–calibrated in regular intervals.

We also report on the non–linear scintillation response studies. In order to reach the saturation regime , we use a weakly focused electron beam to increase the peak charge density by more than two orders of magnitude compared to previous saturation studies[25]. In contrast to Ref. 25, we see saturation starting at peak charge densities in the order of nC/mm². This is about three order of magnitude higher than current charge densities reached in lwfa–experiments. Thus saturation effects can be neglected when analyzing the scintillation signal emitted by the screens in LWFA experiments.

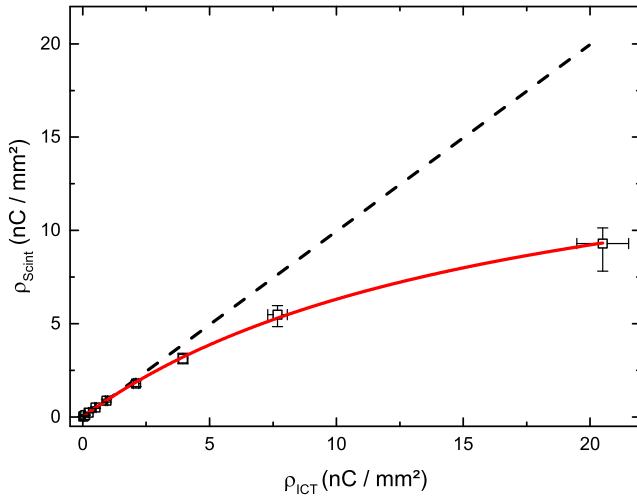Additionally the long term stability for a selected type

FIG. 4. Response function of Kodak Biomax MS showing saturation: The peak charge density emitted by the screen vs. the peak charge density calculated from the beam profile of the scintillator and the charge information given by the ICT. The bunch profile shows a significant saturation towards higher charges. The measured data is fitted with Birk's law of saturation (red line, see eq.2). The black dotted line indicates $\rho_{Scint} = \rho_{ICT}$.
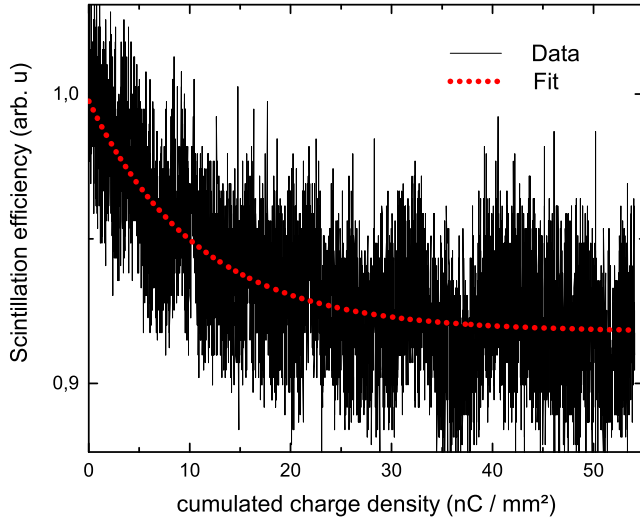

FIG. 5. Long term performance test with Konica Minolta: The screen was irradiated constantly for 1.5 h with 1 Hz repetition rate, 100 pC charge and a spot size of 6 mm² at FWHM. The data was fitted with an exponential decay function. The decay of the photon signal during this experiment was 9%.

of screen was tested. To our knowledge this has never been performed before but is important in order to determine whether the calibration values remain valid over time. We show that a realistic dose of irradiation leads to a significant decrease of the fluorescence efficiency. This artificial aging effect can already occur in the electron detector of plasma accelerators and should be taken into account. Therefore refreshing the scintillation screens reg-
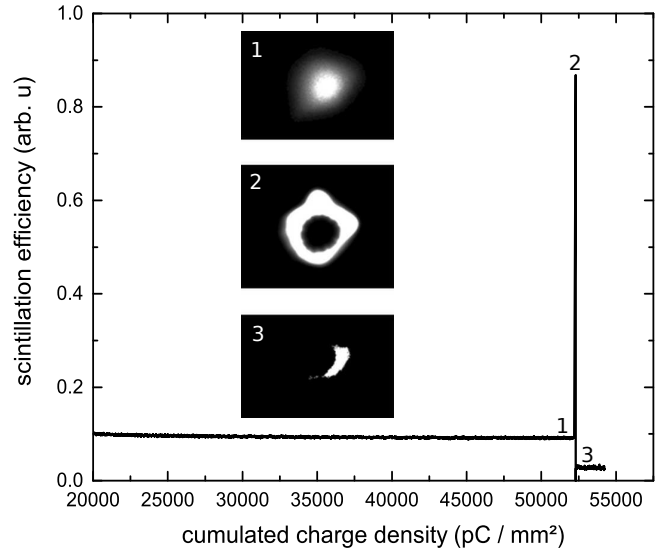

FIG. 6. Damage of Konica Minolta during long term test: The data was taken at a different run with equal parameters than presented in Fig. 5. After applying a cumulative dose of $\approx 52 \, nC/mm^2$ the screen exhibits a bright peak and is permanently damaged afterwards. Due to a lack of heat dissipation in vacuum a the behavior can be explained by thermal melting in the active layer of the scintillator.

ularly is recommended. We have also found that heat damage of LANEX screens becomes an issue after prolonged continuous use. Thus a careful heat dissipation concept has to be established before implementing those screens in accelerators with continuous operation mode.

[1] T. Tajima and J. M. Dawson, Phys. Rev. Lett. **43**, 267 (1979).
[2] U. Schramm, M. Bussmann, A. Irman, M. Siebold, K. Zeil, D. Albach, C. Bernert, S. Bock, F. Brack, J. Branco, J. Couperus, T. Cowan, A. Debus, C. Eisenmann, M. Garten, R. Gebhardt, S. Grams, U. Helbig, A. Huebl, T. Kluge, A. Köhler, J. Krämer, S. Kraft, F. Kroll, M. Kuntzsch, U. Lehnert, M. Loeser, J. Metzkes, P. Michel, L. Obst, R. Pausch, M. Rehwald, R. Sauerbrey, H. Schlenvoigt, K. Steiniger, and O. Zarini, J. J. Phys. Conf. Ser. **874**, 012028 (2017).
[3] E. W. Gaul, M. Martinez, J. Blakeney, A. Jochmann, M. Ringuette, D. Hammond, T. Borger, R. Escamilla, S. Douglas, W. Henderson, G. Dyer, A. Erlandson, R. Cross, J. Caird, C. Ebbers, and T. Ditmire, Appl. Opt. **49**, 1676 (2010).
[4] C. G. R. Geddes, C. S. Toth, J. Van Tilborg, E. Esarey, C. B. Schroeder, D. Bruhwiler, C. Nieter, J. Cary, and W. P. Leemans, Nature **431**, 538 (2004).
[5] J. Faure, Y. Glinec, A. Pukhov, S. Kiselev, S. Gordienko, E. Lefebvre, J.-P. Rousseau, F. Burgy, and V. Malka, Nature **431**, 541 (2004).
[6] S. P. D. Mangles, C. D. Murphy, Z. Najmudin, a. G. R. Thomas, J. L. Collier, a. E. Dangor, E. J. Divall, P. S. Foster, J. G. Gallacher, C. J. Hooker, D. a. Jaroszynski, a. J. Langley, W. B.

Mori, P. a. Norreys, F. S. Tsung, R. Viskup, B. R. Walton, and K. Krushelnick, Nature **431**, 535 (2004).

[7]W. P. Leemans, a. J. Gonsalves, H. S. Mao, K. Nakamura, C. Benedetti, C. B. Schroeder, C. Tóth, J. Daniels, D. E. Mittelberger, S. S. Bulanov, J. L. Vay, C. G. R. Geddes, and E. Esarey, Phys. Rev. Lett. **113**, 1 (2014).

[8]C. B. Schroeder, C. Tóth, B. Nagler, a. J. Gonsalves, K. Nakamura, C. G. R. Geddes, E. Esarey, S. M. Hookert, and W. P. Leemans, Conf. Proc. - Lasers Electro-Optics Soc. Annu. Meet. **2**, 538 (2007).

[9]X. Wang, R. Zgadzaj, N. Fazel, Z. Li, S. A. Yi, X. Zhang, W. Henderson, Y.-Y. Chang, R. Korzekwa, H.-E. Tsai, C.-H. Pai, H. Quevedo, G. Dyer, E. Gaul, M. Martinez, a. C. Bernstein, T. Borger, M. Spinks, M. Donovan, V. Khudik, G. Shvets, T. Ditmire, and M. C. Downer, Nat. Commun. **4**, 1988 (2013).

[10]Y. F. Li, D. Z. Li, K. Huang, M. Z. Tao, M. H. Li, J. R. Zhao, Y. Ma, X. Guo, J. G. Wang, M. Chen, N. Hafz, J. Zhang, and L. M. Chen, Cit. Phys. Plasmas **24**, 023108 (2017).

[11]A. Jochmann, A. Irman, M. Bussmann, J. P. Couperus, T. E. Cowan, A. D. Debus, M. Kuntzsch, K. W. D. Ledingham, U. Lehnert, R. Sauerbrey, H. P. Schlenvoigt, D. Seipt, T. St??hlker, D. B. Thorn, S. Trotsenko, A. Wagner, and U. Schramm, Phys. Rev. Lett. **111**, 114803 (2013).

[12]N. D. Powers, I. Ghebregziabher, G. Golovin, C. Liu, S. Chen, S. Banerjee, J. Zhang, and D. P. Umstadter, Nat. Photonics **8**, 28 (2014).

[13]K. Ta Phuoc, S. Corde, C. Thaury, V. Malka, A. Tafzi, J. P. Goddet, R. C. Shah, S. Sebban, and A. Rousse, Nat. Photonics **6**, 308 (2012).

[14]G. Sarri, D. J. Corvan, W. Schumaker, J. M. Cole, A. Di Piazza, H. Ahmed, C. Harvey, C. H. Keitel, K. Krushelnick, S. P. D. Mangles, Z. Najmudin, D. Symes, A. G. R. Thomas, M. Yeung, Z. Zhao, and M. Zepf, Phys. Rev. Lett. **113**, 224801 (2014).

[15]H.-P. Schlenvoigt, K. Haupt, A. Debus, F. Budde, O. Jäckel, S. Pfotenhauer, H. Schwoerer, E. Rohwer, J. G. Gallacher, E. Brunetti, R. P. Shanks, S. M. Wiggins, and D. A. Jaroszynski, Nat. Phys. **4**, 130 (2007).

[16]M. Fuchs, R. Weingartner, A. Popp, Z. Major, S. Becker, J. Osterhoff, I. Cortrie, B. Zeitler, R. Hörlein, G. D. Tsakiris, U. Schramm, T. P. Rowlands-Rees, S. M. Hooker, D. Habs, F. Krausz, S. Karsch, and F. Grüner, Nat. Phys. **5**, 826 (2009).

[17]A. R. Maier, A. Meseck, S. Reiche, C. B. Schroeder, T. Seggebrock, and F. Grüner, Phys. Rev. X **2**, 031019 (2012).

[18]K. Steiniger, M. Bussmann, R. Pausch, T. Cowan, A. Irman, A. Jochmann, R. Sauerbrey, U. Schramm, and A. Debus, J. Phys. B At. Mol. Opt. Phys **47**, 234011 (2014).

[19]A. Martinez De La Ossa, J. Grebenyuk, T. Mehrling, L. Schaper, and J. Osterhoff, Phys. Rev. Lett. **111**, 245003 (2013).

[20]A. Martinez de la Ossa, T. J. Mehrling, L. Schaper, M. J. V. Streeter, and J. Osterhoff, Phys. Plasmas **22**, 093107 (2015).

[21]K. A. Tanaka, T. Yabuuchi, T. Sato, R. Kodama, Y. Kitagawa, T. Takahashi, T. Ikeda, Y. Honda, and S. Okuda, Rev. Sci. Instrum. **76** (2005), 10.1063/1.1824371.

[22]S. Masuda, E. Miura, K. Koyama, and S. Kato, Rev. Sci. Instrum. **79**, 083301 (2008).

[23]K. Zeil, S. D. Kraft, A. Jochmann, F. Kroll, W. Jahr, U. Schramm, L. Karsch, J. Pawelke, B. Hidding, and G. Pretzler, Rev. Sci. Instrum. **81**, 013307 (2010).

[24]T. Bonnet, M. Comet, D. Denis-Petit, F. Gobet, F. Hannachi, M. Tarisien, M. Versteegen, and M. M. Aleonard, Rev. Sci. Instrum. **84** (2013), 10.1063/1.4775719.

[25]A. Buck, K. Zeil, A. Popp, K. Schmid, A. Jochmann, S. D. Kraft, B. Hidding, T. Kudyakov, C. M. S. Sears, L. Veisz, S. Karsch, J. Pawelke, R. Sauerbrey, T. Cowan, F. Krausz, and U. Schramm, Rev. Sci. Instrum. **81**, 033301 (2010).

[26]R. Morlotti, M. Nikl, M. Piazza, and C. Boragno, J. Lumin. **72-74**, 772 (1997).

[27]B. Hidding, G. Pretzler, M. Clever, F. Brandl, F. Zamponi, A. Lübcke, T. Kämpfer, I. Uschmann, E. Förster, U. Schramm, R. Sauerbrey, E. Kroupp, L. Veisz, K. Schmid, S. Benavides, and S. Karsch, Rev. Sci. Instrum. **78**, 083301 (2007).

[28]Y. Glinec, J. Faure, A. Guemnie-Tafo, V. M. Monard, J. P. Larbre, V. De Waele, J. L. Marignier, M. Mostafavi, V. Malka, and H. Monard, Rev. Sci. Instrum. **77**, 103301 (2006).

[29]G. E. Giakoumakis and D. M. Miliotis, Phys. Med. Biol. **30**, 21 (1985).

[30]K. Nakamura, A. J. Gonsalves, C. Lin, A. Smith, D. Rodgers, R. Donahue, W. Byrne, and W. P. Leemans, Phys. Rev. Accel. Beams **14**, 062801 (2011).